On the Spontaneous Formation of Hydrogen Peroxide in Water Microdroplets

Joseph P. Heindel[1,2], Hongxia Hao[1], R. Allen LaCour[1,2], Teresa Head-Gordon*[1,2,3]

[1]Kenneth S. Pitzer Theory Center and Department of Chemistry
[2]Chemical Sciences Division, Lawrence Berkeley National Laboratory
[3]Departments of Bioengineering and Chemical and Biomolecular Engineering
University of California, Berkeley, CA, 94720 USA
corresponding author: thg@berkeley.edu

Abstract

There is accumulating evidence that many chemical reactions are accelerated by several orders of magnitude in micron-sized aqueous or organic liquid droplets compared to their corresponding bulk liquid phase. However, the molecular origin of the enhanced rates remains unclear as in the case of spontaneous appearance of 1 µM hydrogen peroxide in water microdroplets. In this letter we consider the range of ionization energies and whether interfacial electric fields of a microdroplet can feasibly overcome the high energy step from hydroxide ions (OH^-) to hydroxyl radicals ($OH^\bullet$) in a primary H_2O_2 mechanism. We find that the vertical ionization energies (VIEs) of partially solvated OH^- ions are greatly lowered relative to the average VIE in the bulk liquid, unlike the case of the Cl^- anion which shows no reduction in the VIEs regardless of solvation environment. Overall reduced hydrogen-bonding and under-coordination of OH^- are structural features that that are more readily present at the air-water interface, where the energy scale for ionization can be matched by statistically probable electric field values.

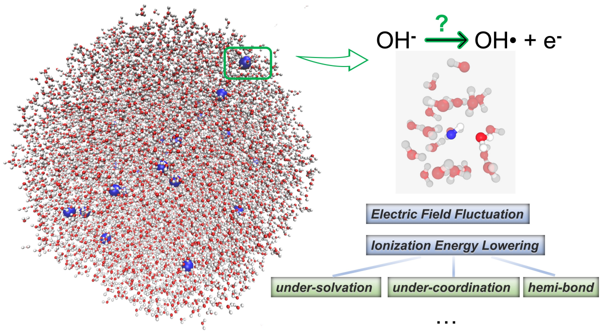

TOC graphic

Microdroplet chemistry refers to the burgeoning experimental evidence of enhanced rates of both organic oxidation and reduction reactions in microdroplets relative to the bulk aqueous phase.[1–3] It is proposed that the underlying features of microdroplet reaction acceleration is the presence of an interface, the presence of hydroxide ions (OH^-) (presumably due to autodissociation of water), and a proposed mechanism that the reduction reactions are driven by loss of an electron from OH^-, that in turn creates OH radicals ($OH^\bullet$) that serve as a strong oxidative agent.

One fundamental example pertains to whether there is spontaneous production of H_2O_2 in aqueous microdroplets, and if so, if it is a feature of the air-water interface.[4–6] Although there are still important disagreements to settle regarding the experimental techniques used to create water droplets, and the concentrations of H_2O_2 actually produced, we do note that both the Zare and Mishra laboratories find detectable amounts of ($\approx$ 1μM) H_2O_2 using gas nebulization and ultrasonic humidification.[3,7] The primary proposed mechanism is that H_2O_2 formation in water microdroplets proceeds spontaneously through the loss of an electron from hydroxide anions followed by radical recombination of $OH^\bullet$ as shown in Eq. 1.

$$H_2O \longrightarrow H^+ + OH^- \tag{1a}$$
$$OH^- \longrightarrow OH^\bullet + e^- \tag{1b}$$
$$2\,OH^\bullet \longrightarrow H_2O_2 \tag{1c}$$

But in order for such a mechanism to be plausible, one must first explain how the microdroplet environment overcomes the highly unfavorable ionization energy step in Eq. 1b. In this work we investigate this rate limiting step by considering whether the interfacial environment can reduce the highly unfavorable vertical ionization energy (VIE) of hydroxide ions found in the bulk aqueous phase (over ~200 kcal/mole)[8]. We also evaluate the VIE for the chloride ion in order to compare it to recent work by the Herbert group that found almost no interfacial effect on the ionization energies of atomic anions compared to the bulk. Their work reached the broad conclusion that the air-water interface is "banal" in regards VIEs of anions[9], e.g. no different than the bulk phase, thereby casting doubt on the plausibility of the mechanism proposed in Eq. 1.

We address these questions with *ab initio* SCS-UMP2 calculations of the VIE of hydroxide ions in a range of water environments. We have chosen to use SCS-UMP2 for the VIE calculations because MP2 is known to describe water cluster data for neutral[10,11], cationic[12], protonated[13], and hydroxide-water systems[14] very accurately. The spin-component scaled version of UMP2 is selected for its superior agreement with the CCSD(T)/aug-cc-pVQZ ionization energy of bare OH^- and is appropriate for open-shell systems. We also compare the VIE for OH^- to Cl^- using SCS-UMP2 and compare it to recent work that found almost no effect on the VIE of atomic anions such as the chloride ion at the air-water interface using hybrid Density Functional Theory.[9] While our main focus is on the energetic barrier associated with ionization of the OH^- and Cl^- anions in a microdroplet environment, we will also briefly discuss the contributions of the solvated electron and other reaction channels to the viability of the reaction mechanism in Eq. (1).

We start with minimized $OH^-(H_2O)_n$ water clusters by increasing the number of water molecules, n, to get a sense of how the VIE converges in nearly ideal hydrogen bonding environments to compare later to thermalized microdroplet configurations. Table 1 provides the VIEs of OH^- using SCS-UMP2 for the gas phase water molecule and optimized $OH^-(H_2O)_n$ cluster minima (n=0-5, 8-17). From Table 1, SCS-UMP2 is found to closely agree with the experimental gas phase VIE

Cluster	$\mathrm{VIE}_{\mathrm{OH}^-}$ (kcal/mol)	$N_{acc.}$
OH^-(gas, experiment)	**42.2**[15]	-
OH^-	43.94	0
$OH^-(H_2O)$	88.93	1
$OH^-(H_2O)_2$	103.76	2
$OH^-(H_2O)_3$	125.01	3
$OH^-(H_2O)_4$	131.69	4
$OH^-(H_2O)_5$	142.94	4
$OH^-(H_2O)_8$	160.99	4
$OH^-(H_2O)_9$	158.40	4
$OH^-(H_2O)_{11}$	167.22	4
$OH^-(H_2O)_{12}$	164.18	4
$OH^-(H_2O)_{13}$	165.85	4
$OH^-(H_2O)_{14}$	172.46	4
$OH^-(H_2O)_{15}$	181.83	4
$OH^-(H_2O)_{16}$	188.56	4
$OH^-(H_2O)_{17}$	186.03	4
OH^-(aqu., experiment)	$\mathbf{207 \pm 15}$[8]	-

Table 1: *Calculated SCS-UMP2/aug-cc-pVTZ vertical ionization energies for a range of water cluster geometries with varying levels of solvation compared to gas and bulk liquid phases from experiment.* The cluster geometries were minimized with MP2/aug-cc-pVTZ, with the exception of the $OH^-(H_2O)_8$ that is minimized with MP2/aug-cc-pVDZ[14].

of 42.2 kcal/mol[16]. Notably, a single optimized hydrogen-bonding interaction for the $OH^-(H_2O)$ dimer doubles the gas phase VIE value, and the increased VIEs of minimized $OH^-(H_2O)_5$ through $OH^-(H_2O)_{17}$ clusters introduce stabilizing interactions that extend beyond the first solvation shell, even though the OH^- ion accepts the same number of hydrogen bonds as in $OH^-(H_2O)_4$.

Ultimately increasing the number of waters of the optimized $OH^-(H_2O)_n$ clusters systematically increases, but does not quite reach, the VIE of ∼207 kcal/mol in the aqueous phase as determined by photoelectron spectroscopy (Table 1).[8] This likely indicates that the gas phase $OH^-(H_2O)_n$ clusters need to be larger and/or include long-ranged electrostatic effects, with the reported evidence suggesting that most anions require on the order of hundreds of solvating water molecules to converge many properties from clusters, including VIE's.[9,17–22]. However, when we extrapolate from the VIE's calculated from the cluster data to the bulk value using linear regression against $n^{-1/3}$, we determine a bulk VIE of 255 kcal/mol that overestimates the bulk experimental value by close to 50 kcal/mol (Supplementary Figure 1). We attribute this to the too ice-like character of the minimized clusters, i.e., not accounting for the weakening of hydrogen bonds due to thermal motion leads to an overestimate of the VIE.

We therefore sampled a range of OH^- water clusters from finite temperature molecular dynamics simulations[23] of a large droplet with a 40 Å radius and containing 24 OH^- and 8614 H_2O molecules using a reactive force field model for water, ReaxFF-CGeM[24,25]. The ReaxFF/C-GeM model has been extensively validated against experiment and theory for small molecules and ions in water[23,26], the water liquid[24], lipid-water interfaces[27], and the air-water interface[23]. From these reactive force field simulations, we extracted clusters of $OH^-(H_2O)_{20}$ which served as the QM region of a

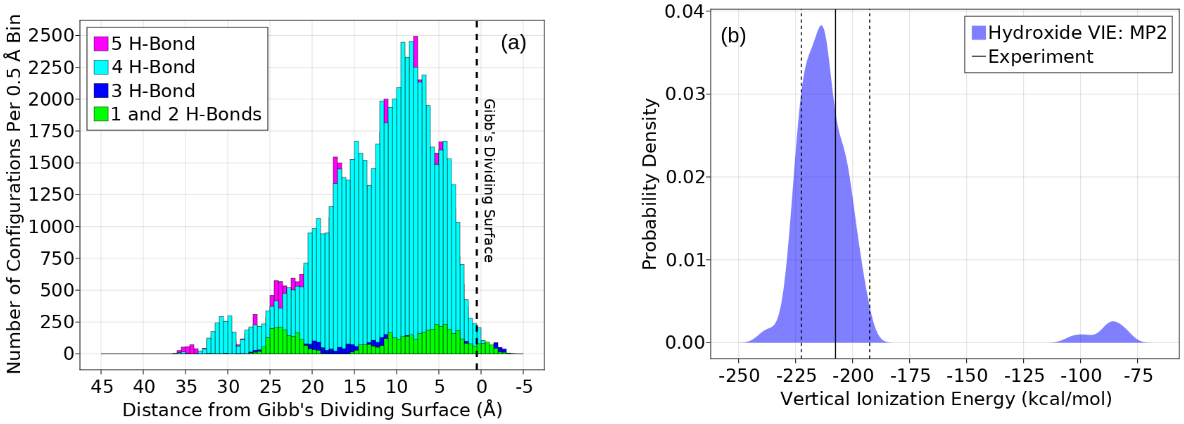

Figure 1: *Structural distributions and water coordination states of OH^- in a 40 Å microdroplet and corresponding vertical ionization energy distributions.* (a) Each distribution is categorized by the number of hydrogen bonds accepted by an OH^-. The dashed line shows the position of the Gibbs dividing surface. (b) distribution of VIE for aqueous OH^- as determined from SCS-UMP2 calculations on $OH^-(H_2O)_{20}$ embedded in the charges of the 1000 nearest neighbor molecules (∼3000 nuclear charges and ∼3000 electronic charges). The solid line shows the bulk value from photoelectron experiments[8]. The dashed lines denote the experimentally reported standard deviations from the Gaussian fit to the photoelectron spectrum.

charge-embedding scheme involving 1000 water molecules (3000 nuclear charges and 3000 electronic charges) in order to calculate the VIE of OH^- in a more realistic bulk environment, as well as evaluating how the VIEs change at the air-water interface where instantaneous fluctuations give rise to large electric field fluctuations[23,28]. Previous studies by Tobias and co-workers have already noted that OH^- and $OH^\bullet$ are favored at the air-water interface by ~ 1 kcal/mol[29,30], supporting the importance of the surface being a distinct feature of microdroplet chemistry for H_2O_2 formation.

Figure 1a shows how the 24 OH^- ions are distributed throughout the water droplet in which a large majority are well solvated with 4-5 hydrogen-bonds, consistent with the well-known hypersolvated structure of the hydroxide ion that contributes to its lower diffusion constant relative to hydronium.[31] However, there is a smaller but significant population of partially solvated OH^- ions, making up ∼7.2% of all the OH^- ions distributed throughout the water droplet. Close to 65% of this small population of under-coordinated configurations lie near or beyond the Gibb's dividing surface, in which OH^- accepts only 1, 2, or 3 hydrogen bonds (see SI for further details). In previous work we have shown that the ReaxFF/CGeM model, in agreement with sum-frequency generation experiments[32,33], predicts that H_3O^+ has a greater propensity for the surface compared to OH^-.[23] Furthermore, the SFG experiments merely show that OH^- does not dramatically perturb the free-OH stretching peak at mM concentrations of OH^-. Thus, it is possible that OH^- is still in the vicinity of the air-water interface without being easily visible in the SFG spectrum. Furthermore, Vogel et al. have observed an excess of OH^- at the air-water interface.[34] Finally, because surface propensities and depletions of small solutes such as OH^- tend to be on the order of 1 kcal/mol or less[29], it is also possible to see fluctuations which bring OH^- to the surface, which is exactly what our simulations show.

We also find that the remaining ∼35% of the small population of OH^- with reduced hydrogen-bonding occurs in the droplet interior, although the coordination number of these same interior OH^-

ions are most often larger by one due to non-hydrogen-bonding neighbors. These configurations likely arise from dynamical defects associated with a changing coordination environment of the OH^- that enables diffusion. Intriguingly, many of these configurations satisfy the geometrical criteria of a hemi-bond which are characterized by close oxygen-oxygen distances.[35–37] We emphasize that OH^- does not actually form a stabilizing interaction with water in the form of a hemi-bond. Instead, the fact that this high-energy arrangement can be sampled is of interest, because upon ionization the radical state can be stabilized by the hemi-bond configuration.

Using these same configurations, Figure 1b reports the VIE distribution from the SCS-UMP2 calculations for the $OH^-(H_2O)_{20}$ clusters and using the charge embedding from the surrounding 1000 water molecules. The agreement between the experimentally measured value of the bulk VIE of 207 ± 15 kcal/mol is in good agreement with our main Gaussian peak position and width at half maximum of 212.9 ± 25.3 kcal/mol. But what is of most interest is that the VIE distribution is bimodal, with a second peak at 89.8 ± 7.3 kcal/mol with a lower bound of ∼66 kcal/mol. This second peak originates almost exclusively from the 1- and 2-coordinated configurations sampled at the air-water interface. This bimodal distribution is also found when using a cluster-continuum model, the Poisson Equation solver (PEqS) developed by the Herbert group,[9,38] and calculated using ωB97M-V/aug-cc-pVDZ level of theory as seen in Supplementary Figure 2.

The gap in the VIE distribution between these two peaks arises from the fact that the hydroxide ion has three lone pairs, so that when OH^- only accepts one or two hydrogen bonds, then there is a set of *2p* electrons which are not strongly stabilized by hydrogen-bonding, resulting in a much lower VIE than one would expect for aqueous OH^-. But when a third hydrogen bond is accepted by OH^-, the VIE jumps nearly all the way to the fully-coordinated average value as already shown with the minimized cluster data (Table 1). This additional low VIE peak integrates to about 3.0% of the total peak area, and therefore its low concentration may not be detectable as a distinct signature in the photoelectron spectrum[8]. A small fraction of the population of low VIEs also arise from the under-coordinated OH^- configurations in the droplet interior, consistent with the idea that hemi-bonded configurations favor low VIEs because they can either destabilize OH^- or stabilize $OH^\bullet$, or both.

Is the OH^- ion different than other atomic ions at the air-water interface? In the work of Paul and Herbert they refer to the "banality" of anion-water hydrogen bonding at the air/water interface which does not differ from the bulk interior, and thus has no distinction in regards the calculated VIEs.[9] We therefore also simulated Cl^- in a large water droplet with ReaxFF/CGeM to see if we reach the same conclusion, again utilizing the same sampling procedure and SCS-UMP2 calculations using a charge embedding scheme. We in fact independently confirm that study in which we see no significant differences in coordination at the air-water interface relative to the inner droplet (Fig. 2a), and therefore the VIE distribution is unimodal with an average and STD of 217.3 ± 24.5 kcal/mol compared to the experimental value of 216.7 ± 8.3 kcal/mol (Fig. 2b). Importantly, there is no effect on VIE depending on undercoordination and/or reduced hydrogen-bonding, and no bimodality in the VIE distributions, which is unlike the OH^- ion as we have shown here.

What are the consequences in regards the lower VIE for a small population of hydroxide ions in undercoordinated water environments? We have recently established that there are average electric fields of ~10 MV/cm at the air-water interface using the ReaxFF/C-GeM model[23], in good agreement with Stark measurements by Min and co-workers using stimulated Raman excited fluorescence microscopy spectroscopy[39]. To illustrate the effect of the stronger surface electric field, the average 89 kcal/mol energy required to ionize OH^- to form $OH^\bullet$ corresponds to a 3.9 V

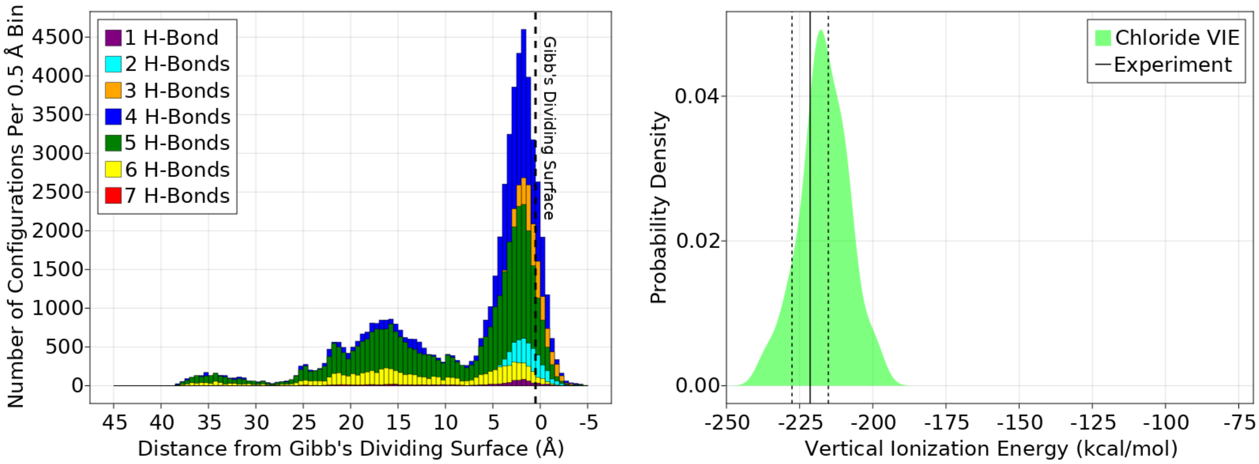

Figure 2: *Structural distributions and water coordination states of Cl^- in a 40 Å microdroplet of NaCl in water and corresponding vertical ionization energy distributions.* (a) Each distribution is categorized by the number of hydrogen bonds accepted by an Cl^-. The dashed line shows the position of the Gibbs dividing surface. (b) the VIE distribution of aqueous Cl^- as determined from SCS-UMP2 calculations on $Cl^-(H_2O)_{20}$ embedded in the 6000 partial charges of the 1000 nearest neighbor water molecules (see Methods). The solid line shows the bulk value from photoelectron experiments[8]. The dashed lines denote the experimentally reported standard deviations from the Gaussian fit to the photoelectron spectrum.

reduction potential. If we assume this potential acts over ~5Å, i.e., the thickness of the air-water interface, that corresponds to an electric field of ∼80 MV/cm which is nearly an order magnitude larger than the estimated electric field average.[23] But due to fluctuations, electric fields exhibit a Lorentzian distribution at the surface for water droplets containing OH^- groups, and hence there is a finite ∼40% probability to have electric field larger than 80 MV/cm. When the electric fields are projected onto the O-H bond of OH^-, which may have variable orientations, there is a smaller but still significant 5% probability to have large enough fields of 80 MV/cm to eject an electron along this bond as per the step in Eq. 1b.

Finally, we return to what is missing in the simple mechanistic picture assumed in Eq. (1) by considering other reactions and experimental factors that could influence this conclusion. For example, in principle, H_2O_2 could also form via the direct ionization of water molecules leading to the formation of a cationic hole $H_2O^{\bullet+}$. However, the IE of H_2O is much higher than that of OH^-, with values as large as 11 eV in the liquid phase[40,41] and 12.6 eV in the gas phase[42]. It is also possible that the relevant process is not ionization, but charge transfer resulting in the production of both H_2O^- and H_2O^+.[43] Another pathway which should be investigated is the effective production of H_2O^+ in two steps. That is, ionization of OH^- and release of a proton from H_3O^+ could be a bimolecular pathway which gives identical products to those observed in oxidative microdroplet reactions[44]. Hence, the analysis reported here could also be relevant to the formation of a cationic hole $H_2O^{\bullet+}$.

One possible limitation in observable H_2O_2 production is that the ionization of OH^- leads to the production of an electron whose fate has not been determined experimentally. If a solvated electron is produced, i.e. it is captured by the droplet, there are reactions which will compete with production of H_2O_2 such as

$$\mathrm{e}^-_{\mathrm{aq}} + \mathrm{H}^+ \longrightarrow \mathrm{H}^\bullet \tag{2a}$$

$$2\,\mathrm{H}^\bullet \longrightarrow \mathrm{H}_2 \tag{2b}$$

$$\mathrm{OH}^\bullet + \mathrm{H}^\bullet \longrightarrow \mathrm{H}_2\mathrm{O} \tag{2c}$$

It is clear from Eq. 2 if an aqueous electron is produced in water (i.e., as proposed in Eq. 1), it will rapidly form $H^\bullet$ by attaching to free hydronium H^+. After production of $H^\bullet$, there are three pathways which quench the $OH^\bullet$ and $H^\bullet$ radicals. Namely, the radicals can produce H_2O_2, H_2, and H_2O. This observation offers two clues: (1) the entire process is pH neutral and (2) one would expect to see production of H_2 gas (which is easy to measure in principle) if it is really the case that this mechanism proceeds through the loss of a solvated electron from OH^-. Finally, there seems to be a consensus that e^-_{aq} has a binding energy of 3.77 eV (87 kcal/mol).[45,46] The implication is that the e^-_{aq} binding energy is commensurate with the VIE of partially solvated OH^- and adds to the plausibility of the Eq. (1) mechanism using thermodynamic arguments.

In conclusion, we have demonstrated that the ionization energy of OH^- is different than atomic anions such as Cl^- when comparing bulk water and the air-water interface. In particular the air-water interface[34] provides an environment for OH^- that makes it more prone to oxidation to the hydroxyl radical with much lower VIE than the bulk phase. For the hydroxide ion the VIE exhibits a bimodal distribution comprised of high IEs for the dominant fully-coordinated configurations of OH^-, with a smaller but non-negligible peak at much lower VIEs that arises from less ideal hydrogen-bonded geometries and reduced nearest neighbor coordination. These under-solvated water configurations are mostly found at the air-water surface, although alternative under-coordinated states involving hemibonds can be found in the microdroplet interior, but in either case they reduce the VIE by half, or more, compared to the VIE's of well-solvated OH^- ions. This is in contrast to Cl^- where the coordination number is largely independent of the location of Cl^- in a microdroplet, and thereby exhibits a unimodal VIE of high energy only. We conclude that the limiting energetic step of hydroxyl radical formation from OH^- corresponds to energy scales that are statistically accessible from available electric fields specific to the air-water interface.[23] Therefore there is a small but still significant probability to spontaneously create H_2O_2 by the mechanism proposed in Eq. 1 on a single microdroplet, and by integrating across many droplets reaching H_2O_2 concentrations above the detection limit reported in experiment.

METHODS

Computational Details of the Reactive Molecular Dynamics Simulation. The snapshots for MP2 calculations were obtained from reactive molecular dynamics simulation of OH^- and Cl^- water solutions using ReaxFF/CGeM.[23,25] In more detail, a 40 Å radius droplet was first created using PACKMOL[47], then equilibrated using molecular dynamics with the AMOEBA force field[48,49] with 1 fs time step for 3 ns within the Tinker-OpenMM platform[50]. This initialized system was then simulated using the ReaxFF/CGeM force field implemented in LAMMPS[25] with a time step of 0.25 fs. After 500 ps of equilibration we collected snapshots every 0.1 ps across a 500 ps production run. The cubic box for the system was set to be $(120\ \text{Å})^3$. All simulations were done in the NVT ensemble at 300K.

In total we sampled 455 extended cluster geometries of the anions from the 500 ps ReaxFF/CGeM production simulations, 114 of which were extracted from the bulk interior and 341 of which were extracted from the air-water interface. These selections overweight anions at the interface, and thus the VIE distributions reported in Figs. 1b and 2b are based on reweighting these 455 VIEs according to the OH^- or Cl^- density distribution determined from the full trajectory. I.e. all VIE computed configurations were assigned a weight based on the probability of finding an anion in a given 0.5 Å radial shell of the droplet. This resampling procedure allows us to generate an unbiased VIE distribution in agreement with Figs. 1a and 2a, although we initially oversampled surface states and undersampled interior states for the VIE calculations.

Computational Details of the MP2 Calculations. We have used SCS-UMP2 for all calculations reported here; the difference between SCS-MP2 and regular MP2 is at most a few kcal/mol in all configurations we analyzed. We have verified that all of the systems ionize the anion as opposed to the surrounding water molecules; the value of $< S^2 >$ is at most 0.759 in all sampled configurations, so spin contamination should be of little concern. We carried out calculations using the full aug-cc-pVTZ basis set on a subset of samples, but found nearly identical results using a mixed basis set approach in which aug-cc-pVTZ is used on the oxygen and hydrogen of hydroxide anions and aug-cc-pVDZ on the surrounding water molecules (Supplementary Table 1). A similar split basis approach was taken by Paul and Herbert in a recent study of VIEs of polyatomic anions.[9] Furthermore, we compared calculations on our configurations using our MP2-based approach and compared it against a hybrid DFT functional used by Paul and Herbert[9] and get excellent agreement (differences around 1 kcal/mol).

We ensure the calculation actually forms $OH^\bullet$ by beginning each calculation from the converged MOs of the gas-phase cluster, which always localized to the right state in our experience. We are able to verify this by checking that the Mulliken spin density is very close to 1.0 on the hydroxyl oxygen atom.

Electrostatic embedding procedure. In the CGeM model[26] there is a Gaussian density placed at the nucleus of each atom with a +1 charge with a corresponding set of electronic shells represented by a Gaussian charge of -1 whose positions are optimized in the field of the nuclei. This has been shown to result in a fast and reliable method of estimating molecular electrostatic potentials.[26,51]

In order to make use of these charges in our UMP2 calculations, we discretize the Gaussian charges into point charges of magnitude +/- 1 which are placed at the center of their respective Gaussians. Hence our system calculations correspond to a QM region of $OH^-(H_2O)_{20}$ in an environment of the nearest 1000 water molecules comprised of ∼6000 point charges (3 for each water x 2 for the positive and negative shells). These charges account for the change in polarization upon ionization by re-optimizing the CGeM shells in both the anionic and radical states, although the polarization is not included self-consistently within the QM wavefunction optimization.Importantly, the charge distribution accurately reflects the instantaneous environment of the OH^- molecule, which is not the case when using continuum methods. Typically, there are about 5874 total embedding charges (maintaining charge neutrality), since some other OH^- ions are within the 1000 nearest neighbors of the OH^- of interest. We neutralize the surrounding environment by not including the extra embedded charges for OH^- molecules in the VIE calculation.

We also compute the VIE for a subset of fully-coordinated and partially-coordinated configurations using a cluster-continuum model, the Poisson Equation solver (PEqS) described elsewhere.[9,38] We use the same approach for discretizing the dielectric function on a grid as in Ref.[9]. The only modification is that the tanh function used to interpolate across the air-water interface is trivially modified to account for the spherical nature of a microdroplet instead of using just the z-coordinate of a grid point as is appropriate when using a slab for simulations. Additionally, we used ωB97M-V/aug-cc-pVDZ when using the PEqS solvation method since otherwise the calculations are too computationally expensive.

While the PEqS model allows for self-consistent inclusion of polarization within the VIE calculation and accounts for differences in dielectric response upon ionization by separating the response into slow and fast modes, the dielectric function is gridded based on the Gibbs dividing surface and hence only includes the average dielectric environment at the surface which may be quite different from the instantaneous environment. Furthermore, how the cavity is constructed is rather arbitrary as it relies on van der Waal's radii for the atoms. The computed VIE is actually rather sensitive to the boundaries of the cavity which introduces a difficult-to-quantify level of uncertainty to these calculations. The results of this comparison are shown in Figure S1.

Hydrogen-bond definitions. We define a hydrogen bond to OH^- geometrically using a 2.7 Å cutoff for the donor-acceptor H−−O distance and 115° for the O−H−−O angle. This definition is chosen since similar definitions are successful in identifying hydrogen bonds generally. Better definitions for H_2O, such as those of Kumar[52], are not designed for OH^- and in some cases depend on the plane of the acceptor H_2O, which does not exist in the case of OH^-. Furthermore, we are primarily concerned with the broad classification based on number of hydrogen bonds, so a different definition may move some structures between neighboring classes, but this will certainly not affect the conclusions of this work. Furthermore, the chosen definition for OH^- seems to do a very good job of separating 2- and 3-coordinated OH^- ions which show the largest difference in VIE. For Cl^-, we use a distance of 2.8 Å and an angle of 130°, which are similar to parameters used by others.[53]

AUTHOR CONTRIBUTIONS

T.H-G. conceived the theme, J.H. formulated the level of theory and performed all ab initio calculations, and H.H. provided electric field estimates. J.H., H.H. and T.H-G. wrote the manuscript, and all authors contributed to all insights through extensive discussion.

SUPPORTING INFORMATION

Additional computational details, materials, and methods. Figure S1 shows an extrapolation to the bulk VIE based on cluster data. Table S1 shows a subset of data in tabular form. Figure S2 directly compares two methods of including long-range polarization, one based on charge embedding and the other based on a polarizable continuum model.

ACKNOWLEDGEMENTS

We thank David Bartels, Dor Ben-Amotz, Graham Cooks, and Son Ngyuen for helpful discussions. We thank the Air Force Office of Scientific Research through the Multidisciplinary University Research Initiative (MURI) program under AFOSR Award No. FA9550-21-1-0170 for the microdroplet chemistry application. The reactive force field work was supported by the National Science Foundation under Grant CHE-1955643. This work used computational resources provided by the National Energy Research Scientific Computing Center (NERSC), a U.S. Department of Energy Office of Science User Facility operated under Contract No. DE-AC02-05CH11231.

CONFLICT OF INTEREST

The authors declare that they have no conflict of interest.

DATA AVAILABILITY

The datasets generated during and/or analyzed during the current study are available from the corresponding author on reasonable request.

CODE AVAILABILITY

The in-house scripts used to generate all data in the manuscript are organized in a private github, but will be made available from the corresponding author on reasonable request.

References

(1) Yan, X.; Bain, R. M.; Cooks, R. G. Organic Reactions in Microdroplets: Reaction Acceleration Revealed by Mass Spectrometry. *Angew. Chem. Int. Ed.* **2016**, *55*, 12960–12972.

(2) Li, Y.; Mehari, T. F.; Wei, Z.; Liu, Y.; Cooks, R. G. Reaction acceleration at air-solution interfaces: Anisotropic rate constants for Katritzky transamination. *J. Mass Spectrom.* **2021**, *56*, e4585.

(3) Zhao, L.; Song, X.; Gong, C.; Zhang, D.; Wang, R.; Zare, R. N.; Zhang, X. Sprayed water microdroplets containing dissolved pyridine spontaneously generate pyridyl anions. *Proc. Natl. Acad. Sci. USA* **2022**, *119*, e2200991119.

(4) Lee, J. K.; Walker, K. L.; Han, H. S.; Kang, J.; Prinz, F. B.; Waymouth, R. M.; Nam, H. G.; Zare, R. N. Spontaneous generation of hydrogen peroxide from aqueous microdroplets. *Proc. Natl. Acad. Sci. USA* **2019**, *116*, 19294–19298.

(5) Lee, J. K.; Han, H. S.; Chaikasetsin, S.; Marron, D. P.; Waymouth, R. M.; Prinz, F. B.; Zare, R. N. Condensing water vapor to droplets generates hydrogen peroxide. *Proc. Natl. Acad. Sci. USA* **2020**, *117*, 30934–30941.

(6) Musskopf, N. H.; Gallo Jr, A.; Zhang, P.; Petry, J.; Mishra, H. The Air–Water Interface of Water Microdroplets Formed by Ultrasonication or Condensation Does Not Produce H2O2. *J. Phys. Chem. Lett.* **2021**, *12*, 11422–11429.

(7) Gallo Jr., A.; Musskopf, N. H.; Liu, X.; Yang, Z.; Petry, J.; Zhang, P.; Thoroddsen, S.; Im, H.; Mishra, H. On the formation of hydrogen peroxide in water microdroplets. *Chem. Sci.* **2022**, *13*, 2574–2583.

(8) Winter, B.; Faubel, M.; Vácha, R.; Jungwirth, P. Behavior of hydroxide at the water/vapor interface. *Chem. Phys. Lett.* **2009**, *474*, 241–247.

(9) Paul, S. K.; Herbert, J. M. Probing interfacial effects on ionization energies: The surprising banality of anion–water hydrogen bonding at the air/water interface. *J. Am. Chem. Soc.* **2021**, *143*, 10189–10202.

(10) Miliordos, E.; Aprà, E.; Xantheas, S. S. Optimal geometries and harmonic vibrational frequencies of the global minima of water clusters (H2O) n, n= 2–6, and several hexamer local minima at the CCSD (T) level of theory. *J. Chem. Phys.* **2013**, *139*, 114302.

(11) Miliordos, E.; Xantheas, S. S. An accurate and efficient computational protocol for obtaining the complete basis set limits of the binding energies of water clusters at the MP2 and CCSD (T) levels of theory: Application to (H2O) m, m= 2-6, 8, 11, 16, and 17. *J. Chem. Phys.* **2015**, *142*, 234303.

(12) Lee, H. M.; Kim, K. S. Dynamics and structural changes of small water clusters on ionization. *J. Comp. Chem.* **2013**, *34*, 1589–1597.

(13) Heindel, J. P.; Yu, Q.; Bowman, J. M.; Xantheas, S. S. Benchmark electronic structure calculations for H3O+ (H2O) n, n= 0–5, clusters and tests of an existing 1, 2, 3-body potential energy surface with a new 4-body correction. *J. Chem. Theo. Comp.* **2018**, *14*, 4553–4566.

(14) Lemke, K. H. Structure and solvation dynamics of the hydroxide ion in ice-like water clusters: a CCSD (T) and car–parrinello molecular dynamics study. *Phys. Chem. Chem. Phys.* **2021**, *23*, 18990–18998.

(15) Rienstra-Kiracofe, J. C.; Tschumper, G. S.; Schaefer, H. F.; Nandi, S.; Ellison, G. B. Atomic and molecular electron affinities: photoelectron experiments and theoretical computations. *Chem. Rev.* **2002**, *102*, 231–282.

(16) Pearson, R. G. Ionization potentials and electron affinities in aqueous solution. *J. Am. Chem. Soc.* **1986**, *108*, 6109–6114.

(17) Coe, J. V. Connecting cluster anion properties to bulk: ion solvation free energy trends with cluster size and the surface vs internal nature of iodide in water clusters. *J. Phys. Chem. A* **1997**, *101*, 2055–2063.

(18) Coe, J. V.; Williams, S. M.; Bowen, K. H. Photoelectron spectra of hydrated electron clusters vs. cluster size: connecting to bulk. *Int. Rev. Phys. Chem.* **2008**, *27*, 27–51.

(19) Cauët, E.; Valiev, M.; Weare, J. H. Vertical ionization potentials of nucleobases in a fully solvated DNA environment. *J. Phys. Chem. B* **2010**, *114*, 5886–5894.

(20) Jacobson, L. D.; Herbert, J. M. A one-electron model for the aqueous electron that includes many-body electron-water polarization: Bulk equilibrium structure, vertical electron binding energy, and optical absorption spectrum. *J. Chem. Phys.* **2010**, *133*, 154506.

(21) Ghosh, D.; Isayev, O.; Slipchenko, L. V.; Krylov, A. I. Effect of solvation on the vertical ionization energy of thymine: From microhydration to bulk. *J. Phys. Chem. A* **2011**, *115*, 6028–6038.

(22) Toth, Z.; Kubecka, J.; Muchova, E.; Slavicek, P. Ionization energies in solution with the QM-QM approach. *Phys. Chem. Chem. Phys.* **2020**, *22*, 10550–10560.

(23) Hao, H.; Leven, I.; Head-Gordon, T. Can electric fields drive chemistry for an aqueous microdroplet? *Nature Comm.* **2022**, *13*, 1–8.

(24) Leven, I.; Hao, H.; Das, A. K.; Head-Gordon, T. A Reactive Force Field with Coarse-Grained Electrons for Liquid Water. *J. Phys. Chem. Lett.* **2020**, *11*, 9240–9247.

(25) Leven, I.; Hao, H.; Tan, S.; Guan, X.; Penrod, K. A.; Akbarian, D.; Evangelisti, B.; Hossain, M. J.; Islam, M. M.; Koski, J. P.; Moore, S.; Aktulga, H. M.; van Duin, A. C. T.; Head-Gordon, T. Recent advances for improving the accuracy, transferability, and efficiency of reactive force fields. *J. Chem. Theo. Comp.* **2021**,

(26) Leven, I.; Head-Gordon, T. C-GeM: Coarse-Grained Electron Model for Predicting the Electrostatic Potential in Molecules. *J. Phys. Chem. Lett.* **2019**, *10*, 6820–6826, PMID: 31613629.

(27) Adams, E. M.; Hao, H.; Leven, I.; Rüttermann, M.; Wirtz, H.; Havenith, M.; Head-Gordon, T. Proton Traffic Jam: Effect of Nanoconfinement and Acid Concentration on Proton Hopping Mechanism. *Angew. Chem. Int. Ed.* **2021**, *60*, 25419–25427.

(28) Willard, A. P.; Chandler, D. Instantaneous Liquid Interfaces. *The Journal of Physical Chemistry B* **2010**, *114*, 1954–1958.

(29) Roeselová, M.; Vieceli, J.; Dang, L. X.; Garrett, B. C.; Tobias, D. J. Hydroxyl radical at the air-water interface. *J. Am. Chem. Soc.* **2004**, *126*, 16308–16309, PMID: 15600317.

(30) Vieceli, J.; Roeselová, M.; Potter, N.; Dang, L. X.; Garrett, B. C.; Tobias, D. J. Molecular dynamics simulations of atmospheric oxidants at the air-water interface: Solvation and accommodation of OH and O3. *J. Phys. Chem. B* **2005**, *109*, 15876–15892, PMID: 16853017.

(31) Liu, R.; Zhang, C.; Liang, X.; Liu, J.; Wu, X.; Chen, M. Structural and dynamic properties of solvated hydroxide and hydronium ions in water from ab initio modeling. *J. Chem. Phys.* **2022**, *157*, 024503.

(32) Das, S.; Imoto, S.; Sun, S.; Nagata, Y.; Backus, E. H.; Bonn, M. Nature of Excess Hydrated Proton at the Water–Air Interface. *Journal of the American Chemical Society* **2019**, *142*, 945–952.

(33) Das, S.; Bonn, M.; Backus, E. H. The surface activity of the hydrated proton is substantially higher than that of the hydroxide ion. *Angew. Chem. Int. Ed.* **2019**, *58*, 15636–15639.

(34) Vogel, Y. B.; Evans, C. W.; Belotti, M.; Xu, L.; Russell, I. C.; Yu, L.-J.; Fung, A. K. K.; Hill, N. S.; Darwish, N.; Gonçales, V. R.; Coote, M. L.; Swaminathan Iyer, K.; Ciampi, S. The corona of a surface bubble promotes electrochemical reactions. *Nature Comm.* **2020**, *11*, 6323.

(35) Rana, B.; Herbert, J. M. Role of hemibonding in the structure and ultraviolet spectroscopy of the aqueous hydroxyl radical. *Phys. Chem. Chem. Phys.* **2020**, *22*, 27829–27844.

(36) Rana, B.; Herbert, J. M. Hidden Hemibonding in the Aqueous Hydroxyl Radical. *J. Phys. Chem. Lett.* **2021**, *12*, 8053–8060.

(37) Chipman, D. M. Hemibonding between hydroxyl radical and water. *J. Phys. Chem. A* **2011**, *115*, 1161–1171.

(38) Coons, M. P.; Herbert, J. M. Quantum chemistry in arbitrary dielectric environments: Theory and implementation of nonequilibrium Poisson boundary conditions and application to compute vertical ionization energies at the air/water interface. *The Journal of chemical physics* **2018**, *148*, 222834.

(39) Xiong, H.; Lee, J. K.; Zare, R. N.; Min, W. Strong Electric Field Observed at the Interface of Aqueous Microdroplets. *J. Phys. Chem. Lett.* **2020**, *11*, 7423–7428, PMID: 32804510.

(40) Mozumder, A. Ionization and excitation yields in liquid water due to the primary irradiation: Relationship of radiolysis with far UV-photolysis. *Phys. Chem. Chem. Phys.* **2002**, *4*, 1451–1456.

(41) Ma, J.; Wang, F.; Mostafavi, M. Ultrafast chemistry of water radical cation, H2O•+, in aqueous solutions. *Molecules* **2018**, *23*, 244.

(42) Page, R. H.; Larkin, R. J.; Shen, Y.; Lee, Y.-T. High-resolution photoionization spectrum of water molecules in a supersonic beam. *J. Chem. Phys.* **1988**, *88*, 2249–2263.

(43) Ben-Amotz, D. Electric buzz in a glass of pure water. *Science* **2022**, *376*, 800–801.

(44) Qiu, L.; Psimos, M. D.; Cooks, R. G. Spontaneous Oxidation of Aromatic Sulfones to Sulfonic Acids in Microdroplets. *J. Am. Soc. Mass Spect.* **0**, *0*, null, PMID: 35312307.

(45) Luckhaus, D.; Yamamoto, Y.-i.; Suzuki, T.; Signorell, R. Genuine binding energy of the hydrated electron. *Sci. Adv.* **2017**, *3*, e1603224.

(46) Nishitani, J.; Yamamoto, Y.-i.; West, C. W.; Karashima, S.; Suzuki, T. Binding energy of solvated electrons and retrieval of true UV photoelectron spectra of liquids. *Sci. Adv.* **2019**, *5*, eaaw6896.

(47) Martínez, L.; Andrade, R.; Birgin, E. G.; Martínez, J. M. PACKMOL: A package for building initial configurations for molecular dynamics simulations. *J. Comp. Chem.* **2009**, *30*, 2157–2164.

(48) Ren, P. Y.; Ponder, J. W. Polarizable atomic multipole water model for molecular mechanics simulation. *J. Phys. Chem. B* **2003**, *107*, 5933–5947.

(49) Laury, M. L.; Wang, L.-P.; Pande, V. S.; Head-Gordon, T.; Ponder, J. W. Revised Parameters for the AMOEBA Polarizable Atomic Multipole Water Model. *The Journal of Physical Chemistry B* **2015**, *119*, 9423–9437.

(50) Harger, M.; Li, D.; Wang, Z.; Dalby, K.; Lagardère, L.; Piquemal, J.-P.; Ponder, J.; Ren, P. Tinker-OpenMM: Absolute and relative alchemical free energies using AMOEBA on GPUs. *J. Comp. Chem.* **2017**, *38*, 2047–2055.

(51) Guan, X.; Leven, I.; Heidar-Zadeh, F.; Head-Gordon, T. Protein C-GeM: A coarse-grained electron model for fast and accurate protein electrostatics prediction. *J. Chem. Inf. Model.* **2021**, *61*, 4357–4369.

(52) Kumar, R.; Schmidt, J.; Skinner, J. Hydrogen bonding definitions and dynamics in liquid water. *J. Chem. Phys.* **2007**, *126*, 05B611.

(53) Pethes, I.; Bakó, I.; Pusztai, L. Chloride ions as integral parts of hydrogen bonded networks in aqueous salt solutions: the appearance of solvent separated anion pairs. *Phys. Chem. Chem. Phys.* **2020**, *22*, 11038–11044.